Optimizing CoCrNi Single Track Geometry in Directed Energy Deposition: A Regression-Based Approach to Laser Power and Scan Speed Control

Available online at www.sciencedirect.com

ScienceDirect

Procedia CIRP 134 (2025) 1035–1040

www.elsevier.com/locate/procedia

Proceedings of the 58th CIRP Conference on Manufacturing Systems 2025

Optimizing CoCrNi Single Track Geometry in Directed Energy Deposition: A Regression-Based Approach to Laser Power and Scan Speed Control

Mohammad Taghian[a,b]*, Federico Mazzucato[c], Anna Valente[c], Abdollah Saboori[a,b]**, Luca Iuliano[a,b]

[a] *Department of Management and Production Engineering, Politecnico di Torino, Corso Duca degli Abruzzi, 24, 10129 Torino, Italy*
[b] *Integrated Additive Manufacturing Center (IAM@PoliTo), Politecnico di Torino, Corso Castelfidardo 51, 10129 Torino, Italy*
[c] *Department of Innovative Technologies, University of Applied Science and Arts of Southern Switzerland (SUPSI), Via La Santa 1, 6962, Lugano, Switzerland*

Corresponding authors. *E-mail address:* *mohammad.taghian@polito.it, **abdollah.saboori@polito.it

Abstract

CoCrNi medium entropy alloys exhibit exceptional mechanical properties, making them ideal for advanced applications in aerospace, biomedical, and energy sectors. This study explores the influence of laser power and scan speed on the track geometry of CoCrNi single tracks produced via Directed Energy Deposition (DED). Second-degree polynomial regression models were developed using a factorial Design of Experiments approach to quantify the relationships between process parameters and track dimensions. Results indicated that laser power and scan speed have a significant impact on track width and height, with increased laser power leading to greater width and moderate scan speeds optimizing height. These insights advance the understanding of CoCrNi in DED processes and aid in parameter optimization for high-performance applications.

Keywords: Additive Manufacturing; Medium Entropy Alloys; Directed Energy Deposition; Melt pool geometry; Regression modeling

1. Introduction

The growing demand for high-performance materials in aerospace, biomedical, and energy industries has spurred the development of novel alloy systems that can withstand extreme environments while maintaining superior mechanical and thermal properties. Medium Entropy Alloys (MEAs), particularly those based on the CoCrNi system, are at the forefront of these developments due to their unique combination of high strength, ductility, and resistance to corrosion and oxidation. The near-equimolar composition of multiple principal elements in MEAs enhances solid solution strengthening, resulting in remarkable thermal stability even at elevated temperatures [1–3]. Despite extensive research on the bulk properties of CoCrNi alloys, their application in advanced Additive Manufacturing (AM) processes—specifically through Directed Energy Deposition (DED)—remains underexplored.

DED, a key AM technology, offers numerous advantages in modern manufacturing, enabling the fabrication of complex geometries, minimizing material waste, and repairing high-value components. By using a high-energy source (such as a laser) to melt and deposit metallic powders layer-by-layer, DED enables high deposition rates and precise control over the manufacturing process, making it particularly suitable for large-scale applications [4,5]. Among various process parameters, laser power and scan speed play crucial roles in determining the geometry of the melt pool, which directly affects the mechanical properties of the deposited material [6,7].

Previous studies on DED have focused on nickel-based superalloys such as IN718 and titanium alloys (e.g., Ti-6Al-

2212-8271 © 2025 The Authors. Published by Elsevier B.V.

10.1016/j.procir.2025.02.227

4V) due to their widespread use in industry. These studies have demonstrated that laser power and scan speed significantly influence the melt pool dimensions—including width, height, and penetration depth—which affect the final part's quality, microstructure, and mechanical properties [8,9]. For instance, increasing laser power generally results in deeper and wider melt pools as more energy is input into the material, leading to greater penetration into the substrate [10]. Conversely, higher scan speeds reduce the interaction time between the laser and the material, often leading to narrower melt pools and less penetration. However, this effect can depend on the specific material and process conditions [11,12].

However, the behavior of multi-principal element alloys such as CoCrNi MEAs in DED remains less understood. The unique thermal properties and solidification behavior of these alloys, which differ from traditional single-component alloys, may result in distinct melt pool dynamics that require specialized process optimization [13,14]. In particular, solid solution strengthening in MEAs and their sluggish diffusion rates can influence how the material responds to heat input, thereby altering the melt pool geometry and solidification process [15]. Empirical studies that focus on single-track deposition, such as the one conducted by Xu et al. on Ti-6Al-4V [16], have shown that melt pool dimensions can be optimized by fine-tuning laser power and scan speed to achieve desired geometries, but similar work for CoCrNi alloys is limited.

The early stages of single-track deposition provide crucial insights into melt pool behavior, allowing for precise control over the deposition process before moving to multi-track and multi-layer structures. Single-track analysis is especially important for novel alloys like CoCrNi, where traditional computational models may not fully capture the complex interactions between the laser and the material. While computational models have been used to predict melt pool dimensions in simpler alloys, they often rely on simplifying assumptions that do not account for the multi-element nature and unique thermal behavior of MEAs. As such, regression models based on empirical data from single-track experiments are essential for developing predictive models that can optimize DED parameters for CoCrNi alloys [17,18].

"This study utilizes regression modeling to assess the impact of laser power and scan speed on the geometry of CoCrNi single tracks fabricated through DED. By analyzing melt pool width, height, penetration depth, and cross-sectional area, this work seeks to establish empirical relationships between process parameters and melt pool geometry. These insights will contribute to the optimization of DED for CoCrNi MEAs, paving the way for improved processing of medium entropy alloys in additive manufacturing and expanding their applicability in high-performance and sustainable industries.

2. Materials and methods

2.1. Material

Single tracks, each 20 mm long, were created using the Prima Additive Laserdyne 430 system, which is equipped with a 1 kW fiber laser and offers a working area of 585 × 400 × 500 mm³. In this study, CoCrNi medium entropy alloy powders were deposited onto a 316L stainless steel substrate with dimensions of 20 × 15 mm and a thickness of 10 mm. The feedstock material consisted of gas-atomized CoCrNi powders, with particle sizes ranging from 20 µm to 150 µm. SEM image of CoCrNi powder particles revealed the presence of small satellite formations and partially melted particles embedded on the powder surfaces, indicative of typical gas atomization characteristics (Fig. 1).

2.2. Experimental Design

Single tracks were deposited using a Design of Experiments (DOE) approach, where two key factors, laser power and scan speed, were varied across three levels. Laser power was varied between 400 W, 500 W, and 600 W, and scan speed was set at 450 mm/min, 600 mm/min, and 750 mm/min. The powder feed rate was kept constant to ensure that only the effect of laser power and scan speed on the track geometry was analyzed. A full factorial design resulted in nine combinations of parameters.

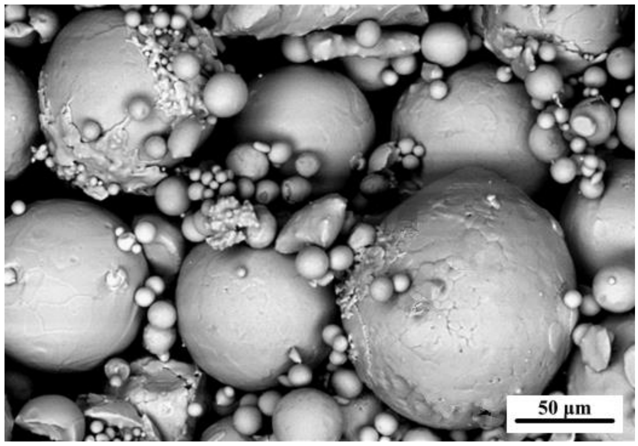

Fig. 1. SEM image of CoCrNi alloy powder particles.

Table 1. DOE factors and levels used in the experiment.

Sample Code	Laser Power P (*W*)	Scan Speed v (mm/min)
1	400	450
2	400	600
3	400	750
4	500	450
5	500	600
6	500	750
7	600	450
8	600	600
9	600	750

2.3. Analysis and Characterization

The substrates with deposited single tracks were cut into cross-sections using a wire-cutting machine. The metallographic preparation of the tracks began with grinding, using various grades of SiC abrasive paper ranging from #180 to #4000 grit, followed by final polishing with 3 µm and 1 µm diamond pastes. After polishing, the surface was etched with Kaling No.2 etchant to reveal the melt pool features for dimensional measurement. Optical micrographs of the melt pools were captured using an optical microscope, and the key dimensions of the tracks, including track width (W), track height (H), and penetration depth (PD), were measured.

To analyze the data, second-degree polynomial regression models were used to examine the impact of laser power and scan speed on track geometry. The regression models were constructed using ordinary least squares (OLS) regression, incorporating linear and quadratic terms for each factor. The general form of the model is as follows:

$$y = \beta_0 + \beta_1 P + \beta_2 v + \beta_3 P^2 + \beta_4 v^2 \quad (1)$$

Where P is the laser power, v is the scan speed, and β represents the model coefficients. While this approach has been widely applied to materials like 316L and Ti-6Al-4V, it has not yet been systematically applied to CoCrNi under DED [19,20].

3. Results and Discussion

2.4. Production of single tracks

Each single track was successfully deposited following the process parameters specified in Table 1. As shown in Fig. 2, the top views of the single tracks indicate that they were stable and exhibited consistent regularity. The tracks exhibited a consistent width along their length, with no visible macro defects, such as particle agglomeration.

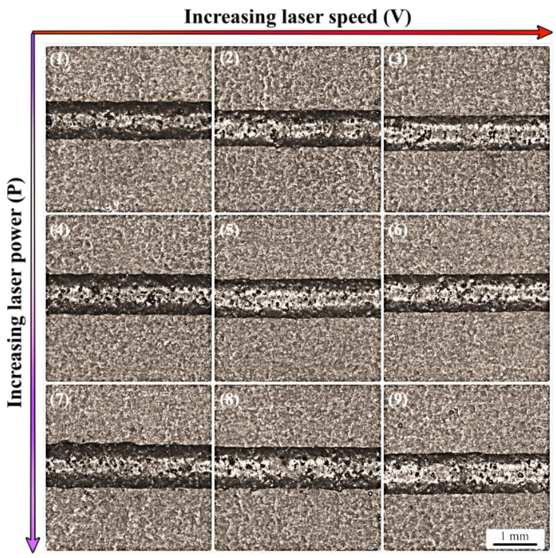

Fig. 2. Top view of CoCrNi single tracks.

The middle section of each track was selected for further analysis to avoid the influence of edge effects. Cross-sections of the single tracks were prepared and examined after a chemical etching process, as shown in Fig. 3. The cross-section analysis revealed good adhesion between the tracks and the substrate, with no visible signs of detachment or discontinuities. The selected process parameters were suitable for producing high-quality single tracks of CoCrNi, confirming their effectiveness in achieving uniform track geometry and stable deposition.

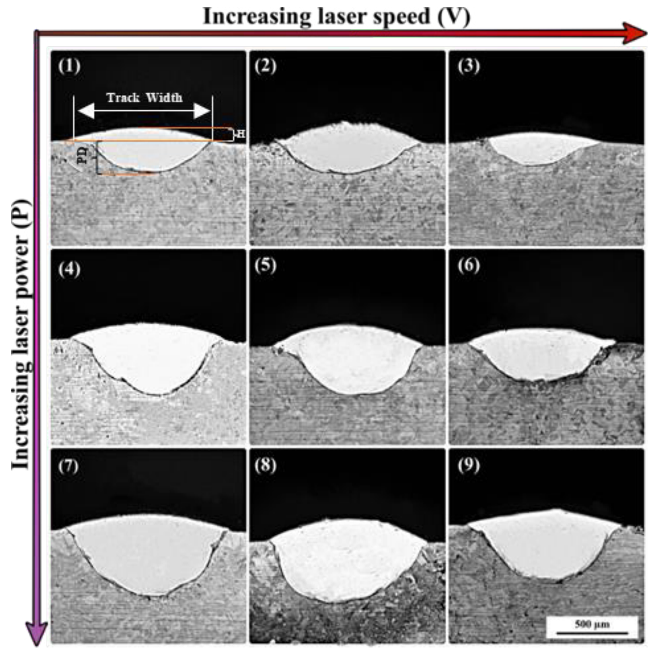

Fig. 3. Cross-section of CoCrNi single tracks.

2.5. Analysis of the track width using Regression modeling

The track width regression model includes linear and quadratic terms for laser power and scan speed to capture non-linear behavior. Equation (2) shows the effect of the laser power and speed on the melt pool width resulting from regression analysis.

$$W = 58.16 + 2.27P - 0.0016P^2 + 0.81v - 0.0008v^2 \quad (2)$$

In this equation, P is the laser power in watts, and v is the scan speed in mm/min. The 3D regression surface plot (Fig. 4) demonstrates that increasing laser power significantly widens the track as the melt pool grows with higher energy input. In contrast, scan speed negatively affects track width: higher speeds shorten the laser-material interaction time, reducing energy input and narrowing the track.

The 3D regression surface plot (Figure 1) demonstrates that increasing laser power significantly widens the track as the melt pool grows with higher energy input. In contrast, scan speed negatively affects track width: higher speeds shorten the laser-material interaction time, reducing energy input and narrowing the track. The regression model for track width has an R-squared value of 93.1%, indicating a high degree of accuracy in explaining the variability of track width based on the laser power and scan speed. The precision of this model is strong, capturing the essential non-linearities of the system. However, slight deviations at extremely high values of laser power and low scan speeds suggest that further refinement or interaction terms could improve the fit at these extremes.

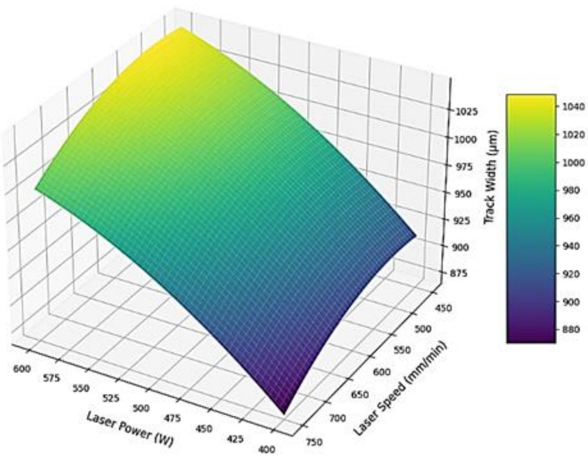

Fig. 4. 3D surface interaction plot for track width.

The regression model for track width has an R-squared value of 93.1%, indicating a high degree of accuracy in explaining the variability of track width based on the laser power and scan speed. The precision of this model is substantial, capturing the essential non-linearities of the system. However, slight deviations at extremely high laser power values and low scan speeds suggest that further refinement or interaction terms could improve the fit at these extremes.

2.6. Regression evaluation of the track height

The regression model for track height follows a similar structure but with more prominent non-linear effects due to the interaction of laser power and scan speed:

$$H = -517.23 + 2.76P - 0.0017P^2 - 0.17v + 0.0000677v^2 \quad (3)$$

Fig. 5. Shows the 3D surface plot for track height (H), illustrating a more complex relationship. Track height increases with laser power up to a threshold (500 W) but then plateaus, indicating that the energy from higher power is primarily distributed laterally rather than vertically. On the other hand, scan speed displays a solid non-linear relationship, where moderate speeds (around 600 mm/min) maximize track height, while high scan speeds reduce the energy input per unit length, limiting vertical growth.

The R-squared value of 96.7% for the track height model indicates excellent precision, demonstrating that the model explains almost all of the variability in track height. This higher R-squared value suggests that the model captures the behavior of track height more accurately than track width, likely because track height is more sensitive to the balance between energy input and material flow dynamics, which the model accounts for through its quadratic terms.

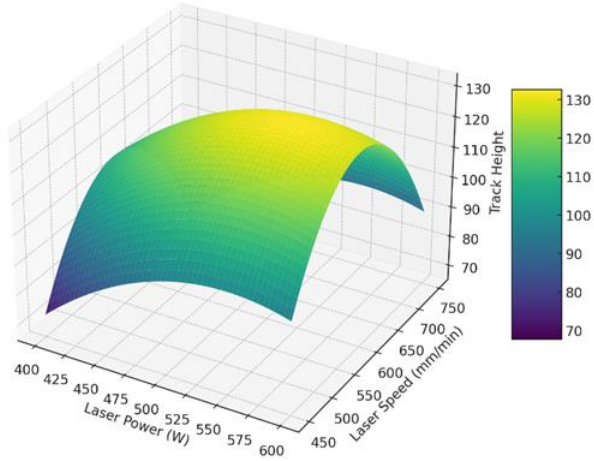

Fig.5. 3D surface interaction plot for track height.

3.3. *Penetration Depth*

The regression model for penetration depth is as follows:

$$PD = 132.45 + 1.82P - 0.0012P^2 + 0.92v - 0.0005v^2 \quad (4)$$

The 3D surface plot for penetration depth (Fig. 6) shows that increasing laser power results in deeper penetration, as expected, due to the increased energy input. Interestingly, the effect of scan speed is more subtle compared to track width and height. The penetration depth slightly increases at lower scan speeds, indicating a more focused energy input in a smaller interaction zone.

The regression model for penetration depth has an R-squared value of 91.5%, which, while still high, is slightly lower than the models for track width and height. This suggests that penetration depth may be influenced by additional factors not fully captured by the current model, such as material flow dynamics or substrate temperature. While the model accurately predicts the general trends, slight deviations at extreme parameter values indicate that further refinement could improve precision.

The interaction term (P·v) was initially included to examine whether laser power and scan speed had a combined effect on penetration depth. However, statistical analysis revealed that this term was insignificant ($p = 0.770$), meaning that adding it did not improve the model's predictive power.

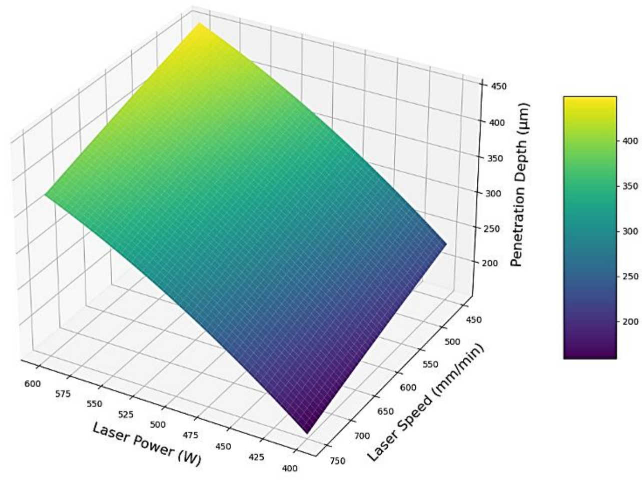

Fig. 6. 3D surface interaction plot for penetration depth.

2.7. Model precision and scientific comparison

The track width model explains 93.1% of the variance, indicating strong predictive power. However, slight deviations at extreme values (high laser power and low scan speed) suggest that further refinements could enhance precision. The track height model performs best, with an R-squared value of 96.7%, showing that it accurately captures the non-linear relationship between laser power and scan speed. This makes track height the most predictable parameter. The penetration depth model has a slightly lower R-squared value of 91.5%, indicating good predictive ability, though somewhat less precise than track width and height. This suggests that additional factors, such as substrate properties or melt pool dynamics, might influence penetration depth.

The melt pool behavior of CoCrNi alloys is strongly influenced by their intrinsic material properties, which differentiate them from other commonly used alloys such as IN718 and Ti-6Al-4V. The observed increase in track width with higher laser power in CoCrNi alloys is attributed to enhanced energy input, leading to a larger melt pool. This effect is supported by the alloy's thermal conductivity, which facilitates efficient heat distribution during the DED process. Additionally, the face-centered cubic (FCC) structure of CoCrNi alloys contributes to their excellent ductility and moderate melting temperature, influencing melt pool dynamics and solidification behavior. The sluggish diffusion effect inherent in medium entropy alloys like CoCrNi further affects the solidification process and final track geometry [21–23].

When compared to IN718 and Ti-6Al-4V, distinct differences emerge. IN718, a nickel-based superalloy, forms wider and deeper melt pools under similar DED parameters due to its lower thermal conductivity and higher density, which enhance heat retention and penetration. In contrast, Ti-6Al-4V exhibits narrower melt pools due to its higher melting point and lower thermal conductivity, which limit heat diffusion and molten pool expansion. These comparisons highlight the unique thermal and physical properties of CoCrNi alloys, which govern their melt pool geometries and solidification characteristics, emphasizing the need for tailored process optimization in DED applications[24,25].

4. Conclusion

This study examined the influence of laser power and scan speed on the key dimensions of CoCrNi single tracks. Multiple tracks were deposited onto a CoCrNi substrate following a design of experiments approach, and track sections were measured to gather dimensional data. Each track was successfully produced, characterized, and analyzed using regression models. The following conclusions were drawn:

- Laser power and scan speed significantly influenced track width, height, and penetration depth. The regression models for each dimension fit well, with the highest precision observed for track height (R-squared = 96.7%).
- The track width model (R-squared = 93.1%) demonstrated high accuracy but indicated that additional interaction effects may need to be explored for even greater precision.
- The penetration depth model (R-squared = 91.5%) was also accurate, though it could benefit from further refinement to capture additional process complexities.
- These regression models offer valuable insights for optimizing DED processes for CoCrNi alloys, providing a foundation for more precise control of track geometry. In the range of process parameters analyzed, these models could be used to estimate the effects of laser power and scan speed, reducing the need for costly experimental trials during process optimization.

Future studies should explore the impact of powder feed rate on track geometry. Additionally, factors like standoff distance, shielding gas flow, and powder particle size should be investigated to enhance process control and optimization.

Acknowledgments

The authors would like to acknowledge Dr. Arashk Memarpour and his colleagues from Höganäs AB (Sweden) for their generous support and provision of resources that enabled this research.

References

[1] B. Cantor, I.T.H. Chang, P. Knight, A.J.B. Vincent, Microstructural development in equiatomic multicomponent alloys, Mater. Sci. Eng. A. 375–377 (2004) 213–218. https://doi.org/10.1016/j.msea.2003.10.257.

[2] B. Gludovatz, A. Hohenwarter, D. Catoor, E.H. Chang, E.P. George, R.O. Ritchie, A fracture-resistant high-entropy alloy for cryogenic applications, Science (80-.). 345 (2014) 1153–1158. https://doi.org/10.1126/science.1254581.

[3] P. Agrawal, S. Thapliyal, S.S. Nene, R.S. Mishra, B.A. McWilliams, K.C. Cho, Excellent strength-ductility synergy in

metastable high entropy alloy by laser powder bed additive manufacturing, Addit. Manuf. 32 (2020) 101098. https://doi.org/10.1016/j.addma.2020.101098.

[4] A. Saboori, A. Aversa, G. Marchese, S. Biamino, M. Lombardi, P. Fino, Application of Directed Energy Deposition-Based Additive Manufacturing in Repair, Appl. Sci. 9 (2019). https://doi.org/10.3390/app9163316.

[5] T. DebRoy, H.L. Wei, J.S. Zuback, T. Mukherjee, J.W. Elmer, J.O. Milewski, A.M. Beese, A. Wilson-Heid, A. De, W. Zhang, Additive manufacturing of metallic components – Process, structure and properties, Prog. Mater. Sci. 92 (2018) 112–224. https://doi.org/https://doi.org/10.1016/j.pmatsci.2017.10.001.

[6] A.J. Pinkerton, L. Li, An analytical model of energy distribution in laser direct metal deposition, Proc. Inst. Mech. Eng. Part B J. Eng. Manuf. 218 (2004) 363–374. https://doi.org/10.1243/095440504323055498.

[7] J.P. Oliveira, A.D. LaLonde, J. Ma, Processing parameters in laser powder bed fusion metal additive manufacturing, Mater. Des. 193 (2020) 1–12. https://doi.org/10.1016/j.matdes.2020.108762.

[8] D.D. Gu, W. Meiners, K. Wissenbach, R. Poprawe, Laser additive manufacturing of metallic components: materials, processes and mechanisms, Int. Mater. Rev. 57 (2012) 133–164. https://doi.org/10.1179/1743280411Y.0000000014.

[9] K. Yuan, W. Guo, P. Li, J. Wang, Y. Su, X. Lin, Y. Li, Influence of process parameters and heat treatments on the microstructures and dynamic mechanical behaviors of Inconel 718 superalloy manufactured by laser metal deposition, Mater. Sci. Eng. A. 721 (2018) 215–225. https://doi.org/https://doi.org/10.1016/j.msea.2018.02.014.

[10] J. Romano, L. Ladani, M. Sadowski, Laser Additive Melting and Solidification of Inconel 718: Finite Element Simulation and Experiment, Jom. 68 (2016) 967–977. https://doi.org/10.1007/s11837-015-1765-1.

[11] Z. Li, J. Chen, S. Sui, C. Zhong, X. Lu, X. Lin, The microstructure evolution and tensile properties of Inconel 718 fabricated by high-deposition-rate laser directed energy deposition, Addit. Manuf. 31 (2020) 100941. https://doi.org/https://doi.org/10.1016/j.addma.2019.100941.

[12] K.P. Monroy, J. Delgado, L. Sereno, J. Ciurana, N.J. Hendrichs, Effects of the Selective Laser Melting manufacturing process on the properties of CoCrMo single tracks, Met. Mater. Int. 20 (2014) 873–884. https://doi.org/10.1007/s12540-014-5011-0.

[13] Y.K. Kim, M.S. Baek, S. Yang, K.A. Lee, In-situ formed oxide enables extraordinary high-cycle fatigue resistance in additively manufactured CoCrFeMnNi high-entropy alloy, Addit. Manuf. 38 (2021) 101832. https://doi.org/10.1016/j.addma.2020.101832.

[14] J.M. Park, J. Choe, H.K. Park, S. Son, J. Jung, T.S. Kim, J.H. Yu, J.G. Kim, H.S. Kim, Synergetic strengthening of additively manufactured (CoCrFeMnNi)99C1 high-entropy alloy by heterogeneous anisotropic microstructure, Addit. Manuf. 35 (2020) 101333. https://doi.org/10.1016/j.addma.2020.101333.

[15] K.-Y. Tsai, M.-H. Tsai, J.-W. Yeh, Sluggish diffusion in Co–Cr–Fe–Mn–Ni high-entropy alloys, Acta Mater. 61 (2013) 4887–4897. https://doi.org/https://doi.org/10.1016/j.actamat.2013.04.058.

[16] Y. Xu, D. Zhang, J. Deng, X. Wu, L. Li, Y. Xie, R. Poprawe, J.H. Schleifenbaum, S. Ziegler, Numerical Simulation in the Melt Pool Evolution of Laser Powder Bed Fusion Process for Ti6Al4V, Materials (Basel). 15 (2022). https://doi.org/10.3390/ma15217585.

[17] A. Bandyopadhyay, B. Heer, Additive manufacturing of multi-material structures, Mater. Sci. Eng. R Reports. 129 (2018) 1–16. https://doi.org/https://doi.org/10.1016/j.mser.2018.04.001.

[18] C. Gullipalli, N. Thawari, A. Chandak, T. Gupta, Statistical Analysis of Clad Geometry in Direct Energy Deposition of Inconel 718 Single Tracks, J. Mater. Eng. Perform. 31 (2022) 6922–6932. https://doi.org/10.1007/s11665-022-06736-1.

[19] Y. He, C. Montgomery, J. Beuth, B. Webler, Melt pool geometry and microstructure of Ti6Al4V with B additions processed by selective laser melting additive manufacturing, Mater. Des. 183 (2019) 108126. https://doi.org/https://doi.org/10.1016/j.matdes.2019.108126.

[20] Z. Sun, W. Guo, L. Li, In-process measurement of melt pool cross-sectional geometry and grain orientation in a laser directed energy deposition additive manufacturing process, Opt. Laser Technol. 129 (2020) 106280. https://doi.org/https://doi.org/10.1016/j.optlastec.2020.106280.

[21] P. Xue, L. Zhu, P. Xu, Y. Ren, B. Xin, G. Meng, Z. Yang, Z. Liu, Research on process optimization and microstructure of CrCoNi medium-entropy alloy formed by laser metal deposition, Opt. Laser Technol. 142 (2021) 107167. https://doi.org/https://doi.org/10.1016/j.optlastec.2021.107167.

[22] Y.-X. Chen, J.-R. Qiu, W.-L. Chang, Y.-K. Hwang, S.-J. Hwang, Process optimization and mechanical properties analysis of Inconel 718/stainless steel 316 L multi-material via direct energy deposition., Sci. Rep. 14 (2024) 28927. https://doi.org/10.1038/s41598-024-80350-0.

[23] T. Li, H. Chen, Y. Huang, Q. Hao, H. Ma, Z. Zhou, S. Li, Y.-D. Wang, Enhanced strength and ductility in (CoCrNi)92Mo2Al6 medium entropy alloy via dual heterogeneous structures, Mater. Res. Lett. 12 (2024) 895–902. https://doi.org/10.1080/21663831.2024.2399579.

[24] M. Khorasani, A. Ghasemi, M. Leary, L. Cordova, E. Sharabian, E. Farabi, I. Gibson, M. Brandt, B. Rolfe, A comprehensive study on meltpool depth in laser-based powder bed fusion of Inconel 718, Int. J. Adv. Manuf. Technol. 120 (2022) 2345–2362. https://doi.org/10.1007/s00170-021-08618-7.

[25] C. Groden, K.D. Traxel, A. Afrouzian, E. Nyberg, A. Bandyopadhyay, Inconel 718-W7Ni3Fe bimetallic structures using directed energy deposition-based additive manufacturing, Virtual Phys. Prototyp. 17 (2022) 170–180. https://doi.org/10.1080/17452759.2022.2025673.